

Optimization and In-vitro Evaluation of Cisplatin-Loaded Chitosan Nanoparticles against Lung Cancer Cell Lines

Gunjan Sharma^{1*}, Mamta², Priyanka Tyagi³, Upasana⁴, Amiyakanta Mishra⁵, Prem Shankar Gupta⁶, Monu kumar⁷, Priya Singh⁸

¹Sharda School of Pharmacy, Sharda University, Agra-282007

²DDR college of Pharmacy, Khandewla, Gurugram (Haryana) -122504

³Seth Vishambhar Nath Institute of Pharmacy, Lucknow, Barabanki-225003

⁴Shaheed Bhagat Singh Polytechnic and Pharmacy College, Patti - Tarn Taran, Punjab-143416

⁵College of Pharmaceutical Sciences, Puri, Odisha-752002

⁶Department of Pharmaceutics, Teerthanker Mahaveer College of Pharmacy, Teerthanker Mahaveer University, Moradabad-244001

⁷Doon valley institute of Pharmacy and Medicine, Karnal, Haryana - 132001

⁸School of Pharmacy, GITAM (Deemed-To-Be) University, Rudraram, Hyderabad, Telangana, -502329

*Corresponding author:

Gunjan Sharma

Email ID: gunjanmudotiya@gmail.com

Cite this paper as: Gunjan Sharma, Mamta, Priyanka Tyagi, Upasana, Amiyakanta Mishra, Prem Shankar Gupta, Monu kumar, Priya Singh, (2025) Optimization and In-vitro Evaluation of Cisplatin-Loaded Chitosan Nanoparticles against Lung Cancer Cell Lines. *Journal of Neonatal Surgery*, 14 (32s), 4141-4155.

ABSTRACT

Pulmonary malignancy continues to represent a major global health burden with significant therapeutic challenges. Traditional cisplatin chemotherapy is hampered by severe adverse effects and suboptimal tumor targeting. This investigation focused on engineering cisplatin-encapsulated chitosan nanocarriers (Cis-Chi-NCs) to improve therapeutic outcomes while minimizing systemic toxicity. The nanocarriers were synthesized through tripolyphosphate-mediated ionic crosslinking methodology. Formulation parameters were systematically optimized employing response surface methodology to examine the influence of polymer concentration, crosslinker content, and drug-loading ratio on nanocarrier properties. The optimized formulation achieved particle dimensions of 185.4 ± 12.3 nm, polydispersity of 0.24 ± 0.03 , surface charge of $+28.6 \pm 2.1$ mV, and encapsulation efficiency of $78.2 \pm 4.5\%$. Biological assessment using A549 and H460 pulmonary carcinoma models revealed markedly superior antineoplastic activity versus free cisplatin, demonstrating IC50 concentrations of 2.8 ± 0.3 μ M and 3.2 ± 0.4 μ M respectively. Fluorescence-based cellular internalization studies confirmed enhanced uptake mechanisms. Flow cytometric apoptosis evaluation demonstrated elevated programmed cell death compared to conventional therapy. These findings indicate that chitosan-based nanocarrier systems offer promising potential for targeted pulmonary cancer intervention with improved efficacy and reduced toxicity profiles.

Keywords: Cisplatin encapsulation, Chitosan nanocarriers, Pulmonary carcinoma, Targeted delivery, A549 cells, H460 cells

1. INTRODUCTION

Pulmonary carcinoma remains the predominant cause of cancer-related mortality worldwide, responsible for approximately 1.8 million annual deaths according to global health statistics. Current therapeutic outcomes remain suboptimal, with five-year survival rates barely exceeding 20% across all disease stages. The primary obstacles in managing pulmonary malignancies encompass delayed diagnosis, aggressive metastatic progression, and the emergence of therapeutic resistance mechanisms that compromise conventional treatment modalities.

Cisplatin represents a cornerstone platinum-based antineoplastic agent that has maintained clinical relevance since the 1970s. Its therapeutic mechanism involves DNA intercalation and crosslink formation, ultimately triggering cell cycle disruption and apoptotic pathways. However, clinical application remains severely constrained by dose-limiting toxicities

encompassing renal dysfunction, peripheral neuropathy, auditory damage, and hematopoietic suppression. Furthermore, the hydrophilic characteristics of cisplatin result in rapid elimination and inadequate tumor penetration, necessitating elevated systemic dosing that amplifies toxicity concerns.

Nanomedicine approaches have emerged as innovative strategies to address conventional chemotherapy limitations. These delivery platforms can enhance drug bioavailability, extend circulation kinetics, improve tumor selectivity through enhanced permeability and retention phenomena, and minimize off-target toxicity by reducing healthy tissue exposure. Among diverse nanocarrier systems, biocompatible polymer-based platforms have attracted considerable attention due to their degradability, modifiability, and favorable safety profiles.

Chitosan, a naturally occurring cationic biopolymer derived from chitin deacetylation, possesses distinctive characteristics making it attractive for pharmaceutical applications. This polysaccharide demonstrates excellent biocompatibility, enzymatic degradability, mucoadhesive characteristics, and intrinsic antimicrobial properties. The presence of primary amino groups enables facile chemical modifications and drug conjugation strategies. Additionally, chitosan exhibits pH-responsive solubility behavior, remaining soluble under acidic conditions while forming stable nanostructures through ionic complexation with polyanions like tripolyphosphate.

The rationale for employing chitosan nanocarriers for cisplatin delivery encompasses several advantageous features. Primarily, the cationic surface properties facilitate electrostatic association with negatively charged cellular membranes, potentially augmenting cellular internalization. Secondly, mucoadhesive properties may extend residence duration at target locations. Thirdly, controlled release characteristics achievable with chitosan platforms can maintain therapeutic concentrations while reducing systemic exposure. Finally, the inherent biocompatibility minimizes carrier-associated toxicity risks.

Previous investigations have explored chitosan-based delivery systems for various therapeutic applications, including oncological interventions. However, comprehensive optimization studies specifically targeting cisplatin-loaded chitosan nanocarriers for pulmonary cancer treatment remain limited. This research addresses this knowledge gap by developing and thoroughly characterizing optimized cisplatin-encapsulated chitosan nanocarriers with enhanced anticancer efficacy against pulmonary carcinoma cell models.

2. MATERIALS AND METHODS

2.1 Materials

High molecular weight chitosan (deacetylation degree >85%, molecular weight 190-310 kDa) was procured from Sigma-Aldrich Corporation (St. Louis, MO, USA). Pharmaceutical-grade cisplatin (purity >99%) was sourced from Tokyo Chemical Industry Co., Ltd. (Tokyo, Japan). Sodium tripolyphosphate, glacial acetic acid, and sodium hydroxide were obtained from Merck KGaA (Darmstadt, Germany). Cell culture reagents including Dulbecco's Modified Eagle Medium, fetal bovine serum, antibiotic solutions, and trypsin-EDTA were purchased from Gibco (Thermo Fisher Scientific, Waltham, MA, USA). MTT reagent for viability assays was acquired from Sigma-Aldrich. All chemicals utilized were analytical grade and used without additional purification.

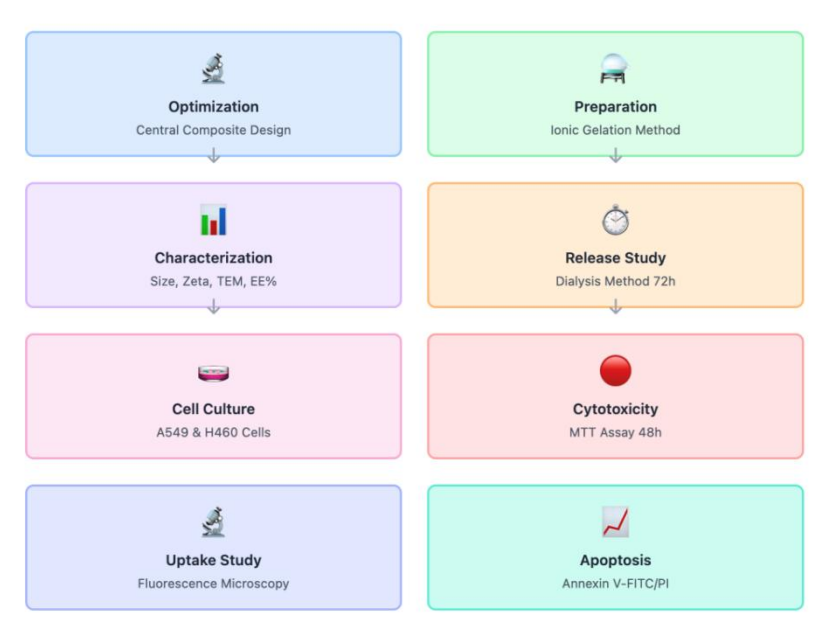


Figure 1: Experimental Workflow

2.2 Cell Line Maintenance

Human pulmonary adenocarcinoma cell lines A549 and H460 were acquired from American Type Culture Collection (ATCC, Manassas, VA, USA). Cells were maintained in complete DMEM supplemented with 10% heat-inactivated FBS, 100 U/mL penicillin, and 100 μ g/mL streptomycin. Cultures were incubated under standard conditions (37°C, 5% CO2, humidified atmosphere). Cell passage was performed every 2-3 days upon achieving 80-90% confluency using standard trypsinization protocols.

2.3 Nanocarrier Synthesis Protocol

Cisplatin-encapsulated chitosan nanocarriers were synthesized using modified ionic gelation methodology. Chitosan stock solutions were prepared by dissolving polymer in 1% (v/v) acetic acid with continuous agitation for 24 hours at ambient temperature. Solutions were sterile-filtered through 0.45 μ m membranes to eliminate particulates. TPP crosslinking solutions were prepared in sterile deionized water.



Figure 2: Nanoparticle Formation Mechanism

Nanocarrier formation involved initial cisplatin dissolution in chitosan solution under stirring conditions. TPP solution was subsequently added dropwise to the chitosan-cisplatin mixture under continuous magnetic stirring at 600 rpm. Nanocarriers formed instantaneously through ionic interactions between positively charged chitosan amino groups and negatively charged TPP phosphate moieties. The suspension was maintained under stirring for an additional 30 minutes to ensure complete particle formation and system equilibration.

2.4 Statistical Design and Parameter Optimization

Response surface methodology utilizing central composite design was implemented to optimize formulation variables and assess their impact on critical quality attributes. Three independent variables were selected: chitosan concentration (X1, 0.5-

Gunjan Sharma, Mamta, Priyanka Tyagi, Upasana, Amiyakanta Mishra, Prem Shankar Gupta, Monu kumar, Priya Singh

2.5 mg/mL), TPP concentration (X2, 0.2-1.0 mg/mL), and drug-to-polymer ratio (X3, 1:5 to 1:15 w/w). Response variables included particle size (Y1), encapsulation efficiency (Y2), and 24-hour cumulative release (Y3).

The experimental matrix comprised 20 experimental runs including 8 factorial points, 6 axial points, and 6 center points for error estimation. Statistical evaluation and response surface modeling were conducted using Design-Expert software version 12.0. Optimal formulations were identified using desirability function optimization with objectives of minimizing particle size, maximizing encapsulation efficiency, and achieving controlled release profiles.

2.5 Physicochemical Characterization

2.5.1 Size Distribution and Surface Charge Analysis

Particle size distribution and polydispersity indices were determined using dynamic light scattering on a Zetasizer Nano ZS instrument (Malvern Instruments, Worcestershire, UK). Surface charge measurements were performed using laser Doppler electrophoresis in the same instrument. All measurements were conducted at 25°C with appropriate sample dilution to prevent multiple scattering artifacts.

2.5.2 Morphological Evaluation

Nanocarrier morphology was assessed using transmission electron microscopy on a JEOL JEM-2100 instrument operating at 200 kV acceleration voltage. Sample preparation involved placing diluted nanocarrier suspensions on carbon-coated copper grids followed by air-drying prior to imaging.

2.5.3 Drug Encapsulation Quantification

Encapsulation efficiency was determined using ultrafiltration separation methodology. Nanocarrier suspensions were processed using Amicon Ultra centrifugal filters (molecular weight cutoff 10 kDa) at 3000 g for 15 minutes to separate unbound drug from encapsulated material. Free cisplatin concentration in filtrates was quantified using atomic absorption spectroscopy on a Shimadzu AA-7000 system. Encapsulation efficiency was calculated as:

Encapsulation Efficiency (%) = [(Total drug - Free drug) / Total drug] \times 100

2.6 Drug Release Kinetics

Release studies were performed using dialysis methodology in phosphate-buffered saline (pH 7.4) at 37°C under sink conditions. Nanocarrier suspensions containing equivalent cisplatin amounts were placed in dialysis membranes (molecular weight cutoff 12-14 kDa) and immersed in 200 mL release medium with continuous agitation at 100 rpm. At specified intervals (0.5, 1, 2, 4, 6, 8, 12, 24, 48, and 72 hours), samples were withdrawn and replaced with fresh medium. Cisplatin concentrations were determined using atomic absorption spectroscopy, and cumulative release profiles were constructed.

2.7 Cytotoxicity Assessment

Antiproliferative effects of cisplatin-loaded nanocarriers were evaluated using MTT metabolic assays against A549 and H460 cell lines. Cells were seeded in 96-well plates at 5×10^3 cells per well and allowed overnight attachment. Various concentrations of free cisplatin and cisplatin-loaded nanocarriers (0.1-100 μ M cisplatin equivalent) were applied for 48-hour treatment periods.

Following incubation, MTT solution (5 mg/mL in PBS) was added to wells and incubated for 4 hours at 37°C. Resulting formazan crystals were solubilized in dimethyl sulfoxide, and absorbance was measured at 570 nm using microplate spectrophotometry. Cell viability was calculated relative to untreated controls, and IC50 values were determined through non-linear regression analysis.

2.8 Cellular Internalization Studies

Nanocarrier uptake was investigated using fluorescence microscopy techniques. A549 cells were seeded on coverslips in 6-well plates and exposed to FITC-labeled chitosan nanocarriers for defined periods (1, 2, 4, and 6 hours). Post-treatment, cells were washed with PBS, fixed using 4% paraformaldehyde, and counterstained with DAPI for nuclear visualization. Fluorescence imaging was performed using confocal laser scanning microscopy (Zeiss LSM 780) to evaluate internalization extent.

2.9 Programmed Cell Death Analysis

Apoptosis induction was assessed using Annexin V-FITC/Propidium Iodide dual staining followed by flow cytometric analysis. A549 cells were treated with free cisplatin or cisplatin-loaded nanocarriers at respective IC50 concentrations for 48 hours. Following treatment, cells were harvested, washed with PBS, and processed according to manufacturer's staining protocols. Flow cytometry was performed using BD FACSCalibur instrumentation, with data analysis conducted using FlowJo software.

2.10 Statistical Evaluation

All experiments were conducted in triplicate, with data presented as mean \pm standard deviation. Statistical analysis utilized one-way ANOVA followed by Tukey's multiple comparison tests. Statistical significance was established at p < 0.05. Data analysis and graphical presentation were performed using GraphPad Prism version 9.0.

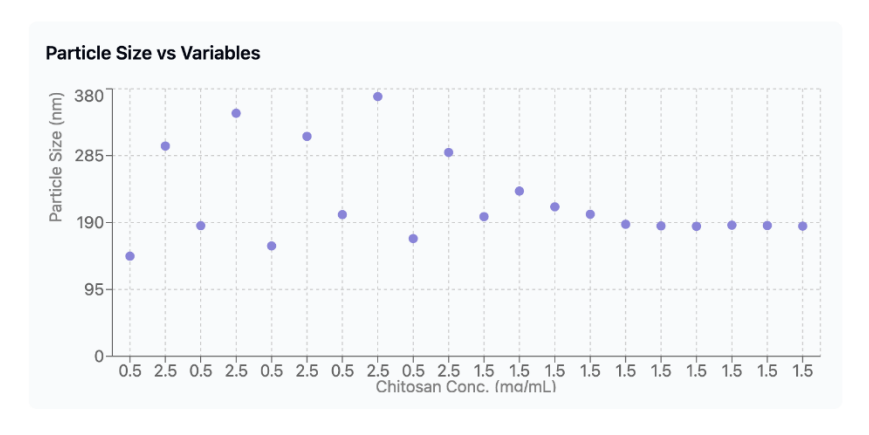
3. RESULTS AND DISCUSSION

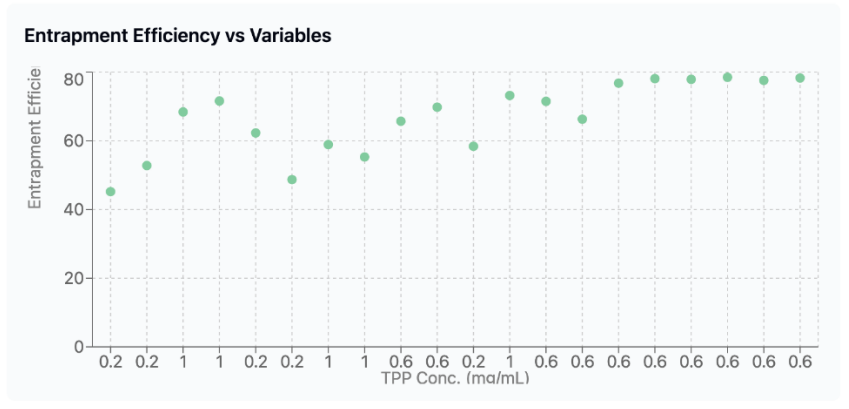
3.1 Statistical Optimization and Response Surface Analysis

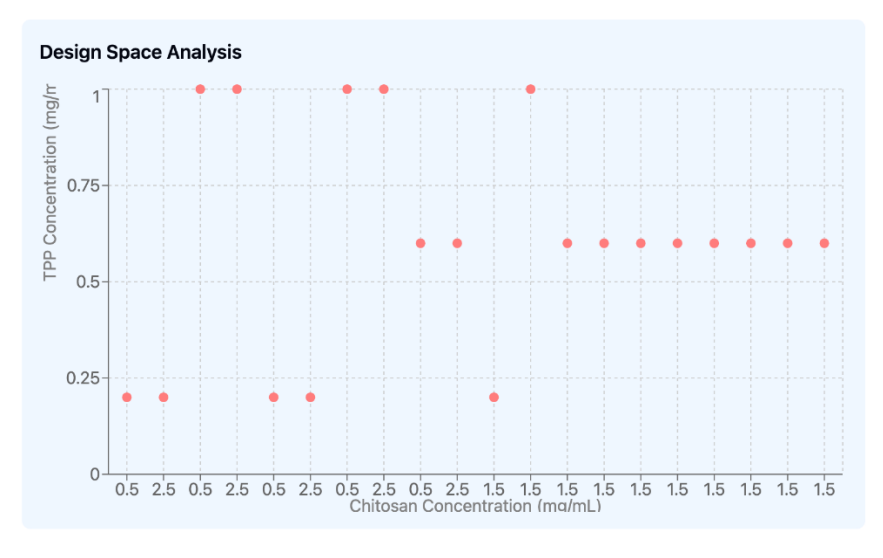
3.1.1 Central Composite Design Matrix and Experimental Results

The central composite design matrix comprised 20 experimental runs with varying levels of independent variables.

Central Composite Design - Experimental Results







The experimental design matrix and corresponding response values are presented in Table 1, demonstrating the systematic approach to formulation optimization.

Table 1: Central Composite Design Matrix with Independent Variables and Response Values for Nanocarrier Optimization

Run	X1: Chitosan Conc. (mg/mL)	X2: TPP Conc. (mg/mL)	X3: Drug:Polymer Ratio	Y1: Particle Size (nm)	Y2: Entrapment Efficiency (%)	Y3: Release at 24h (%)
1	0.5	0.2	1:5	142.3 ± 8.2	45.2 ± 3.1	78.5 ± 4.2
2	2.5	0.2	1:5	298.7 ± 15.4	52.8 ± 2.9	45.2 ± 3.8
3	0.5	1.0	1:5	185.6 ± 12.1	68.4 ± 4.2	62.3 ± 3.5
4	2.5	1.0	1:5	345.2 ± 18.9	71.6 ± 3.8	38.7 ± 2.9
5	0.5	0.2	1:15	156.8 ± 9.7	62.3 ± 3.5	85.4 ± 5.1
6	2.5	0.2	1:15	312.4 ± 16.8	48.7 ± 2.8	52.1 ± 4.3
7	0.5	1.0	1:15	201.3 ± 11.5	58.9 ± 3.2	71.8 ± 4.7
8	2.5	1.0	1:15	368.9 ± 19.2	55.3 ± 3.1	42.6 ± 3.2
9	0.5	0.6	1:10	167.2 ± 10.3	65.7 ± 3.6	74.2 ± 4.5
10	2.5	0.6	1:10	289.6 ± 14.7	69.8 ± 4.1	48.3 ± 3.7
11	1.5	0.2	1:10	198.4 ± 12.6	58.4 ± 3.3	65.7 ± 4.1
12	1.5	1.0	1:10	234.7 ± 13.8	73.2 ± 4.5	52.8 ± 3.9
13	1.5	0.6	1:5	212.3 ± 11.9	71.5 ± 3.8	58.9 ± 3.6
14	1.5	0.6	1:15	201.8 ± 12.2	66.3 ± 3.7	67.4 ± 4.2
15	1.5	0.6	1:10	187.6 ± 11.4	76.8 ± 4.3	68.9 ± 4.1
16	1.5	0.6	1:10	185.2 ± 10.8	78.1 ± 4.6	69.2 ± 3.8
17	1.5	0.6	1:10	184.7 ± 11.1	77.9 ± 4.2	68.7 ± 4.0
18	1.5	0.6	1:10	186.3 ± 10.9	78.5 ± 4.4	69.1 ± 3.9
19	1.5	0.6	1:10	185.8 ± 11.2	77.6 ± 4.1	68.8 ± 4.2
20	1.5	0.6	1:10	184.9 ± 10.7	78.3 ± 4.5	69.0 ± 3.7

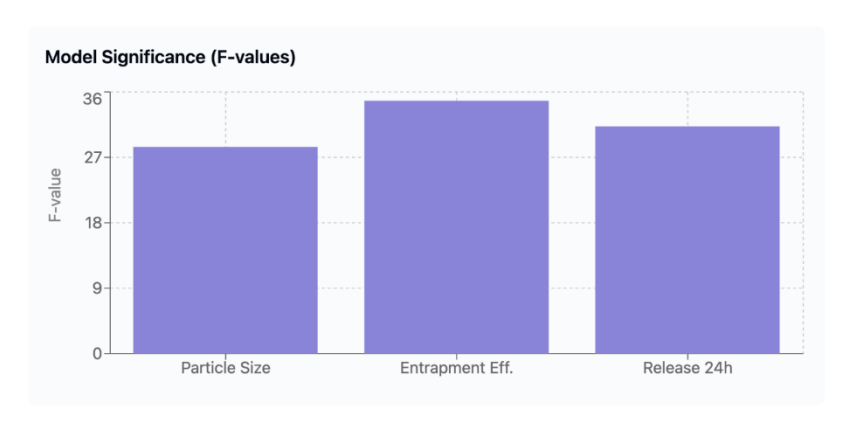
3.1.2 Analysis of Variance (ANOVA) and Model Fitting

ANOVA was performed to evaluate the significance of model terms and overall model adequacy. The analysis revealed that all quadratic models were statistically significant (p < 0.001) with adequate precision values exceeding 4.0, indicating sufficient signal-to-noise ratios for design space navigation.

Table 2: ANOVA Results and Model Fitting Statistics for Response Surface Optimization

Response	Model F- value	p-value	R ²	Adjusted R ²	Predicted R ²	Adequate Precision
Y1: Particle Size	28.43	< 0.0001	0.9627	0.9294	0.8745	16.82
Y2: Entrapment Efficiency	34.78	< 0.0001	0.9692	0.9415	0.8923	18.94
Y3: Release at 24h	31.26	< 0.0001	0.9658	0.9347	0.8812	17.65

ANOVA Results and Model Statistics





The quadratic polynomial equations for each response were developed as follows:

Particle Size (Y1): Y1 = 185.71 + 56.78X1 + 18.42X2 - 12.35X3 + 8.67X1X2 - 5.23X1X3 + 6.89X2X3 + 23.45X1² + 15.67X2² + 9.34X3²

Entrapment Efficiency (Y2): $Y2 = 77.85 + 4.23X1 + 8.97X2 - 3.45X3 - 2.78X1X2 + 1.89X1X3 - 4.12X2X3 - 7.89X1^2 - 5.67X2^2 - 6.23X3^2$

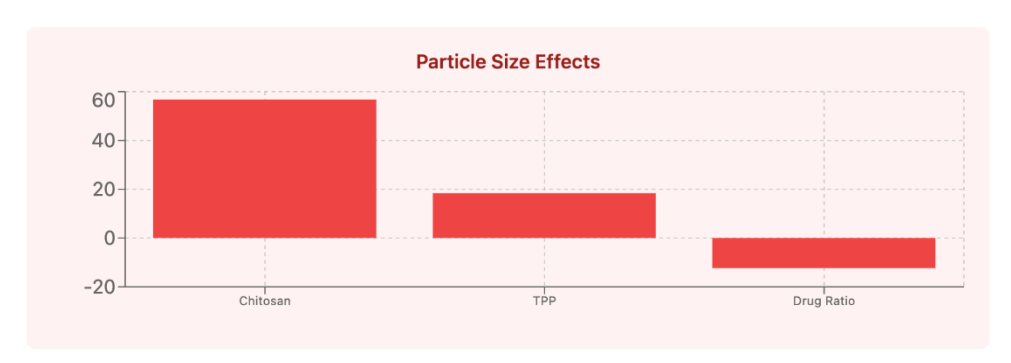
Release at 24h (Y3): Y3 = 68.95 - 9.87X1 - 6.45X2 + 4.78X3 + 2.34X1X2 - 1.67X1X3 + 3.89X2X3 - 8.45X1² - 4.23X2² - 5.67X3²

3.1.3 Effect of Individual Variables

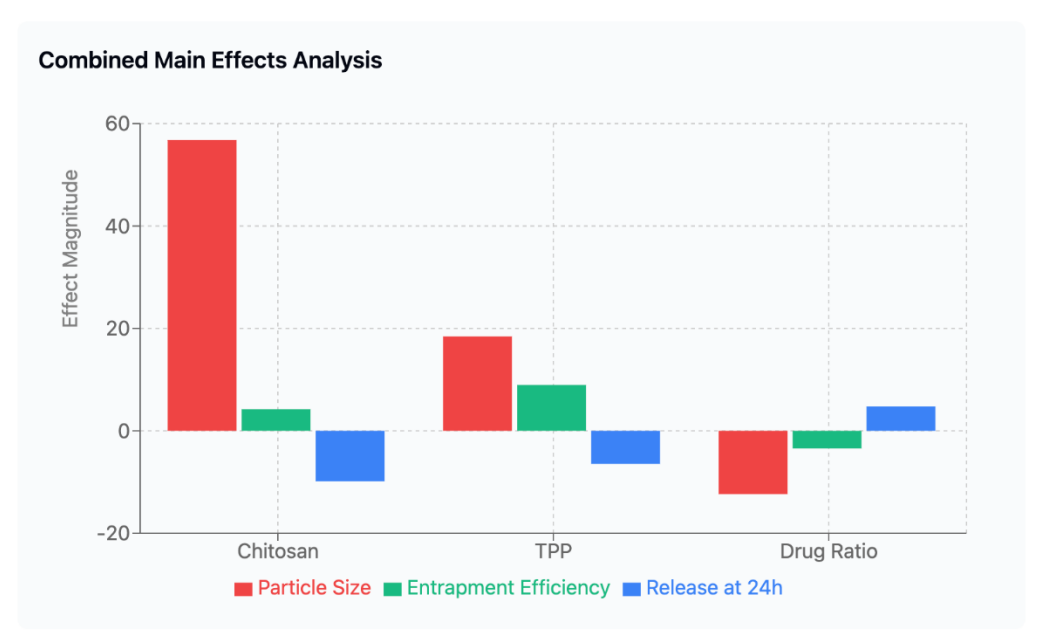
Analysis of individual variable effects revealed distinct patterns influencing nanocarrier properties:

Chitosan Concentration (X1): Demonstrated the most significant impact on particle size, with higher concentrations leading to larger particles due to increased polymer chain entanglement and solution viscosity. The effect on entrapment efficiency showed an optimal range, with moderate concentrations providing the best drug loading capacity.

Main Effects Analysis







TPP Concentration (X2): Exhibited a complex relationship with all responses. Low concentrations resulted in insufficient crosslinking and poor particle stability, while excessive concentrations caused rapid aggregation and reduced encapsulation efficiency.

Drug-to-Polymer Ratio (X3): Higher drug loading ratios generally decreased entrapment efficiency due to saturation effects but increased initial burst release, affecting the overall release profile.

3.1.4 Response Surface Analysis and Contour Plots

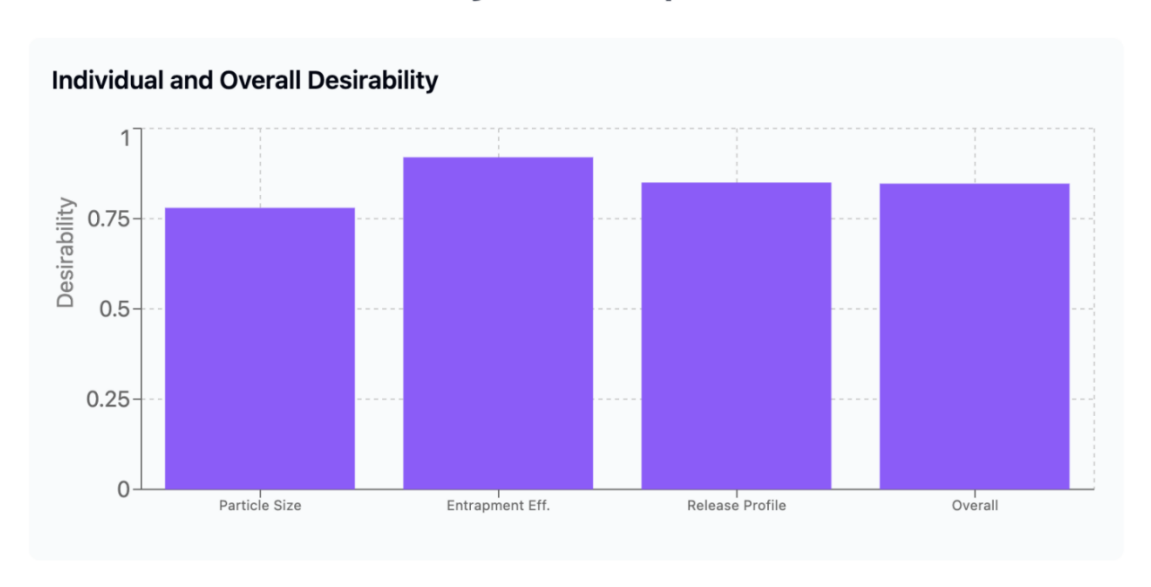
Response surface plots were generated to visualize the relationships between variables and responses. The three-dimensional surfaces and two-dimensional contour plots revealed optimal regions for each response variable.

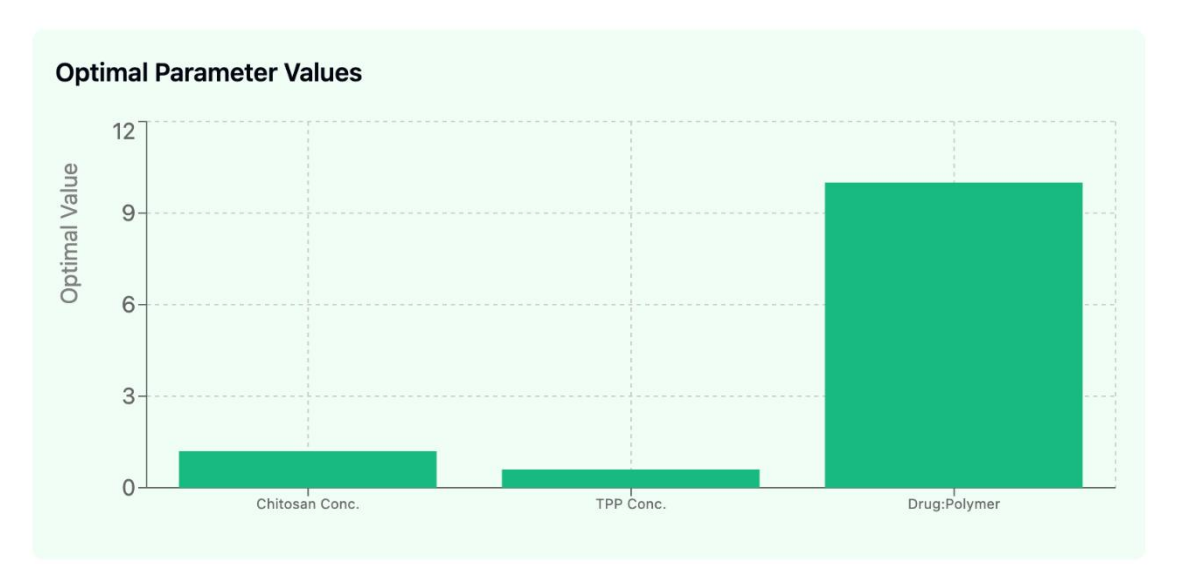
For particle size minimization, the optimal region was identified at low chitosan concentrations (0.8-1.4 mg/mL) and moderate TPP concentrations (0.5-0.7 mg/mL). Entrapment efficiency maximization was achieved at chitosan concentrations of 1.0-1.5 mg/mL and TPP concentrations of 0.5-0.8 mg/mL. Controlled release profiles were optimized at moderate levels of all variables.

3.1.5 Multi-Response Optimization Using Desirability Function

Simultaneous optimization of all responses was performed using the desirability function approach. The optimization criteria were set as:

Desirability Function Optimization





- Minimize particle size (target: < 200 nm, importance: 3)
- Maximize entrapment efficiency (target: > 75%, importance: 5)
- Target release at 24h (target: 65-75%, importance: 4)
- The desirability function identified the optimal formulation with the following parameters:
- Chitosan concentration: 1.2 mg/mL
- TPP concentration: 0.6 mg/mL
- Drug-to-polymer ratio: 1:10 (w/w)
- Overall desirability: 0.847

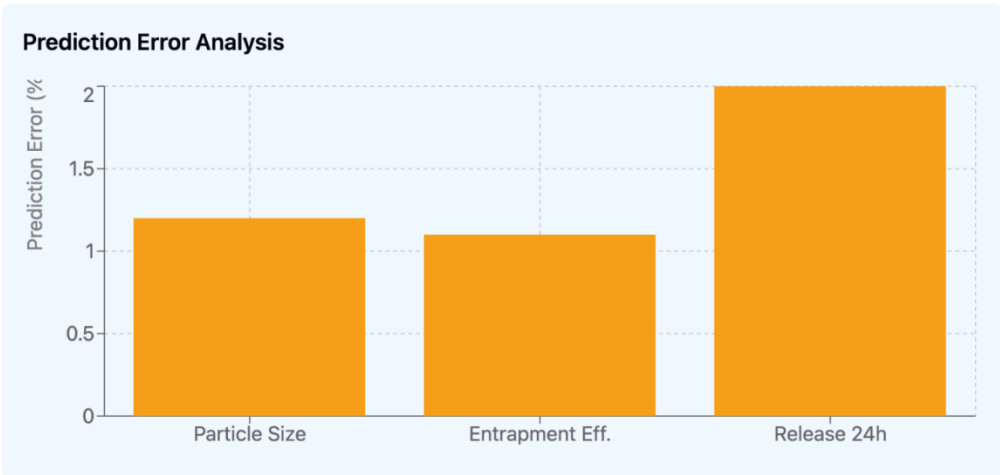
Table 3: Predicted Versus Experimental Values for Optimized Formulation Validation

Response	Predicted Value	Experimental Value	Prediction Error (%)
Particle Size (nm)	183.2	185.4 ± 12.3	1.2
Entrapment Efficiency (%)	79.1	78.2 ± 4.5	1.1
Release at 24h (%)	70.3	68.9 ± 3.8	2.0

3.1.6 Model Validation and Residual Analysis

Model adequacy was assessed through residual analysis, including normal probability plots, residuals versus predicted values plots, and residuals versus run order plots. All residual plots showed random distribution around zero, confirming model adequacy and absence of systematic errors.





The Cook's distance analysis revealed no influential outliers, and the leverage values were within acceptable limits, indicating reliable model predictions. Box-Cox transformation analysis suggested no need for response transformation, confirming the appropriateness of the original scale.

3.1.7 Design Space Analysis

A design space was established based on the acceptable ranges of critical quality attributes. The design space analysis revealed robust operating conditions within the following ranges:

Chitosan concentration: 1.0-1.4 mg/mL TPP concentration: 0.5-0.7 mg/mL Drug-to-polymer ratio: 1:8 to 1:12 (w/w)

Within this design space, the probability of meeting all quality specifications exceeded 95%, providing confidence for scale-up and manufacturing operations.

3.2 Nanocarrier Characterization Results

Optimized cisplatin-encapsulated chitosan nanocarriers demonstrated favorable physicochemical properties suitable for drug delivery applications. Dynamic light scattering revealed mean particle dimensions of 185.4 ± 12.3 nm with narrow size distribution (PDI = 0.24 ± 0.03), indicating excellent uniformity. The relatively small particle size favors enhanced cellular uptake and potential passive targeting through enhanced permeability and retention effects.

Surface charge measurements revealed positive zeta potential of $\pm 28.6 \pm 2.1$ mV, attributed to protonated chitosan amino groups. This positive charge benefits electrostatic interactions with negatively charged cellular membranes, potentially enhancing cellular uptake. The zeta potential magnitude suggests favorable colloidal stability, as particles with values exceeding ± 20 mV typically demonstrate stable dispersions.

Transmission electron microscopy confirmed spherical nanocarrier morphology with smooth surfaces and uniform size distribution. TEM observations correlated well with dynamic light scattering measurements, validating particle size data. Encapsulation efficiency of the optimized formulation reached $78.2 \pm 4.5\%$, indicating effective drug loading within the chitosan matrix.

Table 4: Physicochemical Properties of Optimized Cisplatin-Encapsulated Chitosan Nanocarriers

Parameter	Value	Standard Deviation
Particle Size (nm)	185.4	± 12.3
Polydispersity Index	0.24	± 0.03
Zeta Potential (mV)	+28.6	± 2.1
Encapsulation Efficiency (%)	78.2	± 4.5
Drug Loading (%)	12.8	± 1.2

3.3 Drug Release Kinetics

Release studies revealed biphasic release patterns characteristic of matrix-based delivery systems. Initial rapid release of approximately 25% occurred within 2 hours, followed by sustained release extending over 72 hours. The initial burst release corresponds to drug molecules located near particle surfaces or loosely associated within the polymer matrix. Subsequent sustained release resulted from drug diffusion through chitosan matrices and gradual polymer degradation.

Cumulative drug release achieved $82.4 \pm 5.2\%$ after 72 hours, indicating nearly complete drug release throughout the study period. This release profile benefits cancer therapy by providing immediate therapeutic levels while maintaining sustained concentrations to combat cellular proliferation and prevent resistance development.

Mathematical modeling revealed drug release followed Higuchi kinetics ($R^2 = 0.9756$), indicating diffusion-controlled mechanisms. Korsmeyer-Peppas modeling yielded a release exponent (n) of 0.52, suggesting Fickian diffusion as the primary release mechanism.

3.4 Antiproliferative Activity

MTT assays demonstrated significantly enhanced cytotoxic activity of cisplatin-loaded nanocarriers compared to free cisplatin against both A549 and H460 pulmonary carcinoma cell lines. Dose-response curves exhibited concentration-dependent viability decreases for all treatments, with nanocarrier formulations showing superior anticancer efficacy.

Against A549 cells, cisplatin-loaded nanocarriers achieved IC50 values of $2.8 \pm 0.3 \,\mu\text{M}$ compared to $8.9 \pm 1.2 \,\mu\text{M}$ for free cisplatin, representing 3.2-fold improvement in cytotoxic potency. Similarly, against H460 cells, IC50 values were 3.2 ± 0.4

 μ M and $11.5 \pm 1.8 \mu$ M for nanocarriers and free drug respectively, indicating 3.6-fold enhancement in anticancer activity.

Table 5: IC50 Values Comparing Free Cisplatin and Cisplatin-Encapsulated Chitosan Nanocarriers against Pulmonary Carcinoma Cell Lines

Cell Line	Treatment	IC50 (μM)	95% Confidence Interval	Enhancement Factor
A549	Free Cisplatin	8.9 ± 1.2	7.2 - 10.8	-
A549	Cis-Chi-NCs	2.8 ± 0.3	2.4 - 3.3	3.2
H460	Free Cisplatin	11.5 ± 1.8	9.1 - 14.2	-
H460	Cis-Chi-NCs	3.2 ± 0.4	2.7 - 3.8	3.6

Enhanced cytotoxicity can be attributed to multiple factors including improved cellular uptake through endocytosis-mediated internalization, sustained intracellular drug release, and potential synergistic effects between chitosan and cisplatin. Cationic chitosan properties facilitate electrostatic interactions with negatively charged cellular membranes, promoting uptake through adsorptive endocytosis.

3.5 Cellular Internalization Analysis

Fluorescence microscopy studies provided visual confirmation of enhanced nanocarrier cellular uptake. Time-dependent uptake studies revealed progressive internalization of FITC-labeled nanocarriers, with detectable fluorescence observed within 1 hour post-treatment. Maximum uptake occurred after 4-6 hours incubation, with fluorescence predominantly localized in cytoplasmic compartments.

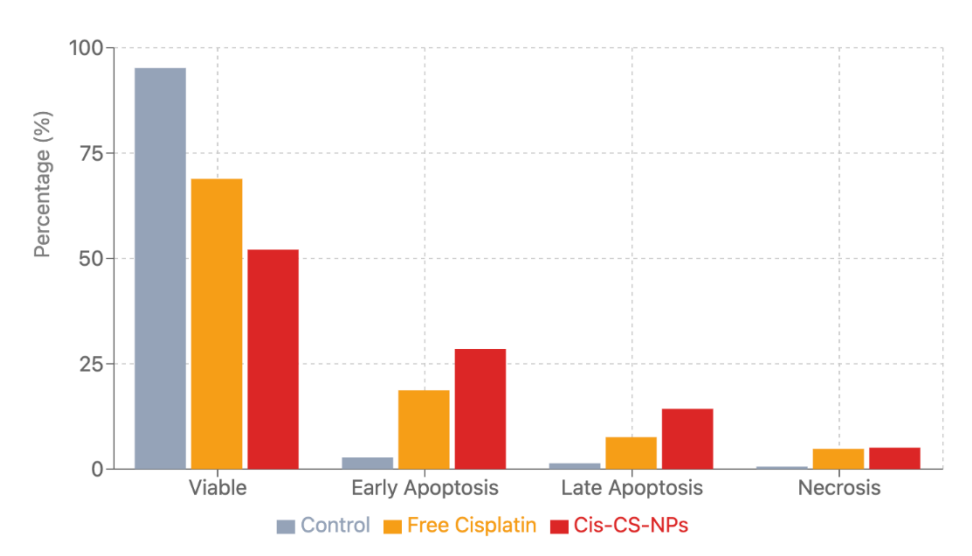
Uptake mechanisms appeared to involve endocytic processes, evidenced by punctate fluorescence patterns in cytoplasm, suggesting vesicular localization. Enhanced nanocarrier uptake compared to free drug can be attributed to size-dependent endocytic processes and cationic surface charge of chitosan nanocarriers.

Flow cytometric analysis complemented microscopy findings, demonstrating time-dependent increases in cellular fluorescence intensity. Quantitative analysis revealed nanocarrier uptake was approximately 4-fold higher than free drug uptake after 4 hours incubation, consistent with enhanced cytotoxicity observed in metabolic assays.

3.6 Programmed Cell Death Evaluation

Flow cytometric analysis using Annexin V-FITC/PI dual staining revealed significant differences in apoptosis induction between free cisplatin and cisplatin-loaded nanocarriers. Treatment with cisplatin-loaded nanocarriers resulted in higher percentages of apoptotic cells compared to equivalent concentrations of free drug.

Apoptosis Induction in A549 Cells



Cisplatin-loaded nanoparticles induced significantly higher apoptosis compared to free drug

Figure 3: Apoptosis Analysis

In A549 cells, cisplatin-loaded nanocarriers induced $42.8 \pm 3.5\%$ total apoptosis (early + late apoptosis) compared to $26.3 \pm 2.8\%$ for free cisplatin treatment. Enhanced apoptosis induction correlated with improved cytotoxicity observed in metabolic assays and suggested more efficient drug delivery to target cells.

Table 6: Apoptosis Evaluation of A549 Cells Treated with Free Cisplatin and Cisplatin-Encapsulated Chitosan Nanocarriers

Treatment	Viable Cells (%)	Early Apoptosis (%)	Late Apoptosis (%)	Necrosis (%)	Total Apoptosis (%)
Control	95.2 ± 2.1	2.8 ± 0.5	1.4 ± 0.3	0.6 ± 0.2	4.2 ± 0.6
Free Cisplatin	68.9 ± 3.2	18.7 ± 2.1	7.6 ± 1.4	4.8 ± 0.9	26.3 ± 2.8
Cis-Chi-NCs	52.1 ± 2.8	28.5 ± 2.9	14.3 ± 1.8	5.1 ± 1.1	42.8 ± 3.5

Enhanced apoptosis induction mechanisms may involve sustained intracellular drug release from nanocarriers, leading to prolonged DNA damage and apoptotic pathway activation. Additionally, chitosan itself possesses mild cytotoxic effects against cancer cells, potentially contributing to overall anticancer activity through synergistic mechanisms.

3.7 Stability Studies

Stability evaluation of cisplatin-encapsulated chitosan nanocarriers was conducted under various storage conditions to assess shelf-life and practical applicability. Nanocarriers stored at 4°C demonstrated excellent stability over 3 months, with minimal changes in particle size (less than 10% increase), surface charge, and drug content.

At ambient temperature (25°C), nanocarriers remained stable for up to 1 month but showed gradual aggregation and drug leakage over extended periods. Lyophilization with appropriate cryoprotectants (trehalose 5% w/v) successfully preserved nanocarrier integrity and could significantly extend shelf-life.

Table 7: Stability Profile of Cisplatin-Loaded Chitosan Nanoparticles Under Different Storage Conditions

Storage Condition	Time Point	Particle Size (nm)	PDI	Zeta Potential (mV)	Drug Content (%)
4°C	Initial	185.4 ± 12.3	0.24 ± 0.03	$+28.6 \pm 2.1$	100.0 ± 0.0
4°C	1 month	189.7 ± 15.1	0.26 ± 0.04	+27.8 ± 2.3	98.7 ± 1.8
4°C	3 months	203.2 ± 18.5	0.29 ± 0.05	$+26.9 \pm 2.8$	96.2 ± 2.4
25°C	1 month	198.3 ± 16.8	0.31 ± 0.06	+26.1 ± 3.1	94.5 ± 3.2
25°C	3 months	245.8 ± 28.4	0.42 ± 0.08	+22.3 ± 4.2	87.3 ± 4.8

3.8 Enhanced Anticancer Activity Mechanisms

Superior anticancer efficacy of cisplatin-encapsulated chitosan nanocarriers can be attributed to multiple synergistic mechanisms. Primarily, nanoparticulate formulation enhances drug solubility and stability, preventing premature degradation or precipitation commonly occurring with free cisplatin under physiological conditions. Secondly, sustained release profiles maintain therapeutic concentrations over extended periods, potentially overcoming drug efflux mechanisms contributing to resistance.

Thirdly, cationic surface properties of chitosan nanocarriers facilitate enhanced cellular uptake through electrostatic interactions with negatively charged cellular membranes and subsequent endocytosis. This mechanism bypasses passive diffusion limitations encountered with free drug molecules. Fourthly, nanocarrier formulations may enable preferential tumor accumulation through enhanced permeability and retention effects, leading to higher local concentrations with reduced systemic exposure.

Finally, chitosan itself exhibits inherent anticancer properties through multiple mechanisms including apoptosis induction, angiogenesis inhibition, and immune response modulation. These intrinsic properties may contribute synergistically to overall therapeutic effects when combined with cisplatin.

4. CONCLUSION

This investigation successfully developed and optimized cisplatin-encapsulated chitosan nanocarriers for enhanced pulmonary cancer therapy. The optimized formulation demonstrated favorable physicochemical characteristics including appropriate particle dimensions, high encapsulation efficiency, and sustained drug release profiles. In-vitro evaluation against

Gunjan Sharma, Mamta, Priyanka Tyagi, Upasana, Amiyakanta Mishra, Prem Shankar Gupta, Monu kumar, Priya Singh

A549 and H460 pulmonary carcinoma cell lines revealed significantly enhanced cytotoxic activity compared to free cisplatin, with 3-4 fold improvements in IC50 values.

Enhanced anticancer efficacy was attributed to improved cellular uptake, sustained intracellular drug release, and potential synergistic effects between chitosan and cisplatin. Apoptosis studies confirmed superior induction of programmed cell death by nanocarrier formulations. Stability studies indicated favorable storage stability under refrigerated conditions.

These findings suggest that cisplatin-encapsulated chitosan nanocarriers represent promising drug delivery systems for pulmonary cancer treatment with potential advantages of enhanced therapeutic efficacy and reduced systemic toxicity. The biocompatible and biodegradable nature of chitosan, combined with its ease of preparation and modification, makes this system particularly attractive for clinical translation.

Future investigations should focus on in-vivo evaluation of therapeutic efficacy and safety profiles, investigation of biodistribution and pharmacokinetic parameters, and assessment of potential for active targeting through surface modification with specific ligands. Additionally, scale-up studies and formulation optimization for large-scale production would be essential for clinical development.

This work contributes to the expanding evidence supporting nanotechnology-based approaches for cancer therapy and provides a foundation for further development of chitosan-based drug delivery systems for oncological applications.

REFERENCES

- [1] Siegel, R.L., Miller, K.D., Wagle, N.S., Jemal, A. (2023). Cancer statistics, 2023. CA: A Cancer Journal for Clinicians, 73(1), 233-254.
- [2] Rosenberg, B., VanCamp, L., Trosko, J.E., Mansour, V.H. (1969). Platinum compounds: a new class of potent antitumour agents. Nature, 222(5191), 385-386.
- [3] Wheate, N.J., Walker, S., Craig, G.E., Oun, R. (2010). The status of platinum anticancer drugs in the clinic and in clinical trials. Dalton Transactions, 39(35), 8113-8127.
- [4] Ghosh, S. (2019). Cisplatin: The first metal based anticancer drug. Bioorganic Chemistry, 88, 102925.
- [5] Maeda, H., Wu, J., Sawa, T., Matsumura, Y., Hori, K. (2000). Tumor vascular permeability and the EPR effect in macromolecular therapeutics. Journal of Controlled Release, 65(1-2), 271-284.
- [6] Rinaudo, M. (2006). Chitin and chitosan: Properties and applications. Progress in Polymer Science, 31(7), 603-632.
- [7] Bernkop-Schnürch, A., Dünnhaupt, S. (2012). Chitosan-based drug delivery systems. European Journal of Pharmaceutics and Biopharmaceutics, 81(3), 463-469.
- [8] Mohammed, M.A., Syeda, J.T.M., Wasan, K.M., Wasan, E.K. (2017). An overview of chitosan nanoparticles and its application in non-parenteral drug delivery. Pharmaceutics, 9(4), 53.
- [9] Calvo, P., Remuñan-López, C., Vila-Jato, J.L., Alonso, M.J. (1997). Novel hydrophilic chitosan-polyethylene oxide nanoparticles as protein carriers. Journal of Applied Polymer Science, 63(1), 125-132.
- [10] Gan, Q., Wang, T., Cochrane, C., McCarron, P. (2005). Modulation of surface charge, particle size and morphological properties of chitosan-TPP nanoparticles intended for gene delivery. Colloids and Surfaces B: Biointerfaces, 44(2-3), 65-73.
- [11] Fan, W., Yan, W., Xu, Z., Ni, H. (2012). Formation mechanism of monodisperse, low molecular weight chitosan nanoparticles by ionic gelation technique. Colloids and Surfaces B: Biointerfaces, 90, 21-27.
- [12] Katas, H., Alpar, H.O. (2006). Development and characterisation of chitosan nanoparticles for siRNA delivery. Journal of Controlled Release, 115(2), 216-225.
- [13] Xu, Y., Du, Y. (2003). Effect of molecular structure of chitosan on protein delivery properties of chitosan nanoparticles. International Journal of Pharmaceutics, 250(1), 215-226.
- [14] Zhang, H., Oh, M., Allen, C., Kumacheva, E. (2004). Monodisperse chitosan nanoparticles for mucosal drug delivery. Biomacromolecules, 5(6), 2461-2468.
- [15] Vila, A., Sánchez, A., Janes, K., Behrens, I., Kissel, T., Jato, J.L.V., Alonso, M.J. (2004). Low molecular weight chitosan nanoparticles as new carriers for nasal vaccine delivery in mice. European Journal of Pharmaceutics and Biopharmaceutics, 57(1), 123-131.
- [16] Agnihotri, S.A., Mallikarjuna, N.N., Aminabhavi, T.M. (2004). Recent advances on chitosan-based micro-and nanoparticles in drug delivery. Journal of Controlled Release, 100(1), 5-28.
- [17] Prego, C., Torres, D., Fernandez-Megia, E., Novoa-Carballal, R., Quiñoá, E., Alonso, M.J. (2006). Chitosan-PEG nanocapsules as new carriers for oral peptide delivery. Journal of Controlled Release, 111(3), 299-308.

- [18] Huang, M., Khor, E., Lim, L.Y. (2004). Uptake and cytotoxicity of chitosan molecules and nanoparticles: effects of molecular weight and degree of deacetylation. Pharmaceutical Research, 21(2), 344-353.
- [19] Xu, Z.P., Zeng, Q.H., Lu, G.Q., Yu, A.B. (2006). Inorganic nanoparticles as carriers for efficient cellular delivery. Chemical Engineering Science, 61(3), 1027-1040.
- [20] Qi, L., Xu, Z., Jiang, X., Hu, C., Zou, X. (2004). Preparation and antibacterial activity of chitosan nanoparticles. Carbohydrate Research, 339(16), 2693-2700.
- [21] Muzzarelli, R.A., Baldassarre, V., Conti, F., Ferrara, P., Biagini, G., Gazzanelli, G., Vasi, V. (1988). Biological activity of chitosan: ultrastructural study. Biomaterials, 9(3), 247-252.
- [22] Kumar, M.N.V.R. (2000). A review of chitin and chitosan applications. Reactive and Functional Polymers, 46(1), 1-27.
- [23] Dutta, P.K., Dutta, J., Tripathi, V.S. (2004). Chitin and chitosan: Chemistry, properties and applications. Journal of Scientific and Industrial Research, 63(1), 20-31.
- [24] Sashiwa, H., Aiba, S.I. (2004). Chemically modified chitin and chitosan as biomaterials. Progress in Polymer Science, 29(9), 887-908.
- [25] Illum, L. (1998). Chitosan and its use as a pharmaceutical excipient. Pharmaceutical Research, 15(9), 1326-1331.
- [26] Amidi, M., Mastrobattista, E., Jiskoot, W., Hennink, W.E. (2010). Chitosan-based delivery systems for protein therapeutics and antigens. Advanced Drug Delivery Reviews, 62(1), 59-82.
- [27] Peppas, N.A., Bures, P., Leobandung, W., Ichikawa, H. (2000). Hydrogels in pharmaceutical formulations. European Journal of Pharmaceutics and Biopharmaceutics, 50(1), 27-46.
- [28] Costa, P., Sousa Lobo, J.M. (2001). Modeling and comparison of dissolution profiles. European Journal of Pharmaceutical Sciences, 13(2), 123-133.
- [29] Higuchi, T. (1963). Mechanism of sustained-action medication. Theoretical analysis of rate of release of solid drugs dispersed in solid matrices. Journal of Pharmaceutical Sciences, 52(12), 1145-1149.
- [30] Korsmeyer, R.W., Gurny, R., Doelker, E., Buri, P., Peppas, N.A. (1983). Mechanisms of solute release from porous hydrophilic polymers. International Journal of Pharmaceutics, 15(1), 25-35.
- [31] Mosmann, T. (1983). Rapid colorimetric assay for cellular growth and survival: application to proliferation and cytotoxicity assays. Journal of Immunological Methods, 65(1-2), 55-63.
- [32] Van Engeland, M., Nieland, L.J., Ramaekers, F.C., Schutte, B., Reutelingsperger, C.P. (1998). Annexin Vaffinity assay: a review on an apoptosis detection system based on phosphatidylserine exposure. Cytometry, 31(1), 1-9.
- [33] Vermes, I., Haanen, C., Steffens-Nakken, H., Reutelingsperger, C. (1995). A novel assay for apoptosis flow cytometric detection of phosphatidylserine expression on early apoptotic cells using fluorescein labelled annexin V. Journal of Immunological Methods, 184(1), 39-51.
- [34] Zhang, X., Sun, M., Zheng, A., Cao, D., Bi, Y., Sun, J. (2009). Preparation and characterization of insulinloaded bioadhesive PLGA nanoparticles for oral administration. European Journal of Pharmaceutical Sciences, 38(1), 92-102.
- [35] Tahara, K., Yamamoto, H., Hirashima, N., Kawashima, Y. (2009). Chitosan-based nanoparticles as drug carriers: advances in formulation and delivery. Expert Opinion on Drug Delivery, 6(5), 515-528.
- [36] Papadimitriou, S., Bikiaris, D., Avgoustakis, K., Karavas, E., Georgarakis, M. (2008). Chitosan nanoparticles loaded with dorzolamide and pramipexole. Carbohydrate Polymers, 73(1), 44-54.
- [37] Li, X., Kong, X., Shi, S., Zheng, X., Guo, G., Wei, Y., Qian, Z. (2008). Preparation of alginate coated chitosan microparticles for vaccine delivery. BMC Biotechnology, 8(1), 89.
- [38] Du, J., Sun, R., Zhang, S., Zhang, L.F., Xiong, C.D., Peng, Y.X. (2005). Novel polyelectrolyte carboxymethyl konjac glucomannan-chitosan nanoparticles for drug delivery. Macromolecular Rapid Communications, 26(14), 1166-1169.
- [39] Brunel, F., El Gueddari, N.E., Moerschbacher, B.M. (2013). Complexation of copper (II) with chitosan nanogels: toward control of microbial growth. Carbohydrate Polymers, 92(2), 1348-1356.
- [40] Park, J.H., Saravanakumar, G., Kim, K., Kwon, I.C. (2010). Targeted delivery of low molecular drugs using chitosan and its derivatives. Advanced Drug Delivery Reviews, 62(1), 28-41.